Biogeosciences
Discussions
EGU
Open Access

Canal blocking optimization in restoration of drained peatlands

Iñaki Urzainki[1,2], Ari Laurén[2], Marjo Palviainen[3], Kersti Haahti[1], Arif Budiman[4], Imam Basuki[4,5], Michael Netzer[4], and Hannu Hökkä[1]

[1]Natural Resources Institute Finland (Luke), Latokartanonkaari 9, FI-00790, Helsinki, Finland
[2]School of Forest Sciences, Faculty of Science and Forestry, University of Eastern Finland, Joensuu Campus, PO Box 111, (Yliopistokatu 7), FI-80101 Joensuu, Finland
[3]University of Helsinki, Department of Forest Sciences, PO-Box 27 00014, Helsinki, Finland
[4]Winrock International, 2121 Crystal Drive, Suite 500, Arlington, VA 22202, USA
[5]Center for International Forestry Research (CIFOR), Situ Gede, Sindang Barang, Bogor 16115, Indonesia

Correspondence: Iñaki Urzainki (inaki.urzainqui@luke.fi)

Abstract. Drained peatlands are one of the main sources of carbon dioxide (CO_2) emissions globally. Emission reduction and, more generally, ecosystem restoration can be achieved by raising the water table using canal or drain blocks. When restoring large areas, the number of blocks becomes limited by the available resources, which raises the following question: in which exact positions should a given number of blocks be placed in order to maximize the water table raise throughout the area? There is neither a simple nor an analytic answer. The water table response is a complex phenomenon that depends on several
5 factors, such as the topology of the canal network, site topography, peat hydraulic properties, vegetation characteristics and meteorological conditions. We developed a new method to position the canal blocks based on the combination of a hydrological model and heuristic optimization algorithms. We applied this approach to a large drained peatland area (931 km^2) in Sumatra, Indonesia. Our solution consistently improved the performance of traditional block locating methods, indicating that drained
10 peatland restoration can be made more effective at the same cost by selecting the positions of the blocks using the presented scheme.

1 Introduction

Peatlands occupy around 3% of global land area, but hold up to one third (630 Pg) of all carbon (C) held in active terrestrial
15 pools (Page et al., 2011; Xu et al., 2018). In pristine conditions, peatlands typically act as C sinks, since the input of dead organic matter is usually greater than the biological decomposition of peat and other organic residues (Reddy and DaLaune, 2008). However, drainage may turn peatlands into C sources (Minkkinen and Laine, 1998; Hooijer et al., 2010; Ojanen et al., 2010; Jauhiainen et al., 2012). Drainage removes excess water from peat and enhances site productivity, which is favourable for agriculture and forest production (Päivänen and Hånell, 2012; Evans et al., 2019). Even though drainage-based bioproduction
20 can be economically viable, it has severe environmental drawbacks: it increases CO_2 emissions (Ojanen et al., 2010; Jauhiainen

et al., 2012), the rate of peat subsidence (Evans et al., 2019), nutrient export to water courses (Nieminen et al., 2017) and fire risk in peatlands (Wösten et al., 2008). CO_2 emissions have been particularly severe in managed tropical peatlands, where the annual CO_2 emission has been as high as $70 - 90$ Mg ha^{-1} (Hooijer et al., 2010; Jauhiainen et al., 2012). In Indonesian agriculture and forestry, plantations on drained peatlands play an important role: agriculture and forestry contribute to about

25 20% of the total national greenhouse gas emissions (World Resources Institute). According to Hooijer et al. (2010), the CO_2 emissions from drained peatlands in Indonesia range from 290 to 700 Tg y^{-1}.

Water table depth (WTD) has been found to be the key variable controlling CO_2 emissions (Hooijer et al., 2010; Wilson et al., 2011; Jauhiainen et al., 2012; Evans et al., 2019). In tropical peatlands, it has been estimated that raising the WTD from -80 to -40 cm would decrease CO_2 emissions on average by 50 Mg ha^{-1} y^{-1} (Jauhiainen et al., 2012) and the rate of peat

30 subsidence by 1.7 cm y^{-1} (Evans et al., 2019). The reason behind the beneficial effects is that increasing water content in peat limits oxygen (O_2) supply for the decomposer organisms, and consequently slows down the rate of aerobic decomposition (Reddy and DaLaune, 2008). Therefore, raising the WTD is a powerful tool for peatland restoration, the aim of which is to establish a self-sustaining peat ecosystem that accumulates C (Päivänen and Hånell, 2012).

WTD raise for peatland restoration has been commonly carried out using drain or canal blocks constructed from surrounding

35 peat material, mineral soil or artificial materials (Armstrong et al., 2009; Parry et al., 2014). As discussed by Parry et al. (2014) the WTD response depends on site topography (Holden et al., 2006), block position (Holden, 2005), drain spacing and the hydraulic characteristics of peat (Dunn and Mackay, 1996). When restoring large peatland areas, the number of blocks becomes easily limited by available resources. This is especially important in tropical peatlands, where the canals are typically large, requiring big constructions that increase the cost of a single block. Working with limited resources raises a natural question:

40 in which exact positions should a given amount of blocks be placed in order to maximize the amount of rewetted peat and consequently to minimize CO_2 emissions and the rate of subsidence?

To the best of our knowledge there is no systematic approach to support finding optimal block positions (Armstrong et al., 2009; Ritzema et al., 2014). Experimentally testing different block positions is impractical and inefficient. Process-based hydrological models, on the other hand, provide a useful tool to reveal changes in the WTD induced by different drainage

45 setups (Dunn and Mackay, 1996). However, for large peatland areas and complex canal networks, process-based models on their own are not sufficient to solve for the best block positions, because the number of possible positions becomes subject to combinatorial explosion. To illustrate this, let us consider a setup with b blocks having n possible locations. The number of ways in which the blocks could be arranged equals $\binom{n}{b}$. For the cases studied in this paper, $n = 11311$ and $b \approx 40$, and thus there are $\binom{11311}{40} = 1.6 \cdot 10^{114}$ ways to place them. Even with powerful computers it is not feasible to find the best combination

50 by exhaustive search; a different strategy is required. Global optimization methods are commonly used to solve combinatorial management problems in engineering and forestry when the variables are discrete and the design spaces are discontinuous and non-convex (Jin et al., 2016; Laurén et al., 2018; Rao, 2009).

Our objective in this work was to build a computational scheme based on a simple hydrological model coupled to an optimization algorithm that maximizes the amount of rewetted peat with a given number of canal blocks. The hydrological

55 model computes WTD as a two-dimensional surface. Using the WTD -a proxy for the CO_2 emissions- as the target variable of

the optimization problem, the optimization algorithm looks for the positions of the blocks that minimize the emissions. This scheme was applied to a drained peatland area (931 km^2) in Sumatra, Indonesia. Topographical details of the peatland areas, as well as rainfall data and physical peat properties were employed in the simulations. The implication of different canal blocking schemes will be discussed in the regional greenhouse gas emission context.

2   Material and Methods

2.1   Computational scheme

The computation consists of the following modules: the canal water level subroutine, the hydrological model and an optimization algorithm. Figure 1 describes a single iteration in the optimization process. The canal water level subroutine computes the canal water level (CWL) that would result from building canal blocks in some given positions. The CWL is passed to the hydrological model, which solves the WTD for the whole area, a quantity that is closely related to the target variable of the optimization problem, $\langle \zeta \rangle$, defined in section 2.1.2. The optimization algorithm evaluates the target variable and decides what canal block configuration to be studied next. This onsets a new iteration loop. We also tested an alternative, simpler optimization approach (SO) that maximizes the change in CWL instead and bypasses the hydrological simulation completely. See Table 1 for definitions of symbols used.

The modeling domain, *i.e.*, the study area, is represented as a 2D grid (raster). In what follows, we will refer as *canal raster* to the set of pixels that form the canal network.

2.1.1   Canal water level subroutine

This subroutine calculates the CWL after building a set of blocks, $\boldsymbol{v}'$, based on their positions, $\boldsymbol{k}$. In the absence of any blocks the CWL is assumed to be at a fixed distance, wd, below the peat surface, s,

$$v_i = s_i - wd, \tag{1}$$

for all i in the canal raster. In our simulations, the value of wd was determined by direct observation and was set to $wd = 1.2\text{m}$. When a block is built in a given pixel of the canal raster its water level raises up to the head level of the block, hl. The CWL in the adjacent pixels further up the canal network will also raise to the same height, as shown in Figure 2.

In order to know how $\boldsymbol{v}$ would be affected by building a block in any pixel of the canal raster, information about the topology of the canal network is needed. The direction of the water flow was captured following two simple rules. For any two pixels in the canal network raster, we say that pixel A is connected to pixel B if and only if:

1. A and B are adjacent to each other (diagonal adjacency is also allowed).

2. A's water level is lower than B's, *i.e.*, $v_A < v_B$.
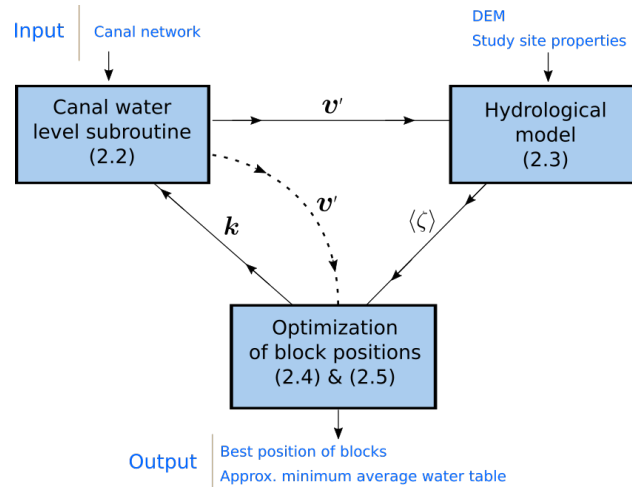
Figure 1. Schematic representation of a single iteration of the computation, showing the most relevant input and output and the interaction between the modules. The numbers in parentheses refer to the corresponding section in the main text. DEM stands for digital elevation model. The optimization algorithm proposes a particular position for the canal blocks, k. Then, the canal water level subroutine computes the CWL resulting from that block placement, v'. This information is passed on to the hydrological model, which solves for the WTD with v' as boundary conditions and computes the resulting target variable, the average WTD over 3 dry days, $\langle \zeta \rangle$, Eq.(7). The optimization algorithm evaluates the performance and proposes a new k according to some rules specific to each algorithm. When using the alternative simple optimization strategy (SO), the CWL change, which depends only on v and v', see Eq.(13), is used as a target variable. This corresponds to the shortcut shown by the dashed arrows.
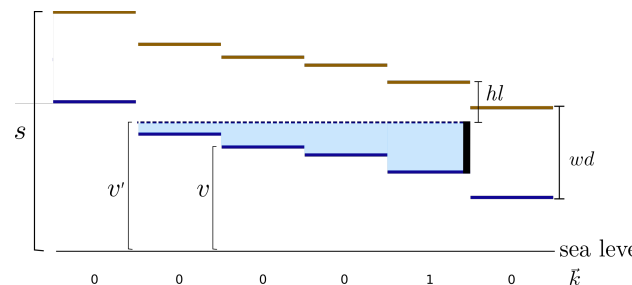
Figure 2. Side view of a canal. The blue and the brown horizontal solid lines represent the initial CWL, v, and the height of the peat surface, s, respectively. wd is a parameter that denotes the distance from the peat surface to the CWL. Each pixel is represented by one line segment. The vertical black line represents the block, and the dotted blue line represents the CWL after the block has been placed, v'. The shaded blue area represents the change in the CWL due to the block. The value of the vector k is $k_i = 1$ if there is a block in pixel i and otherwise $k_i = 0$.

Thus, the pixels affected by building a block in pixel A are located further up the canal network. A detailed description of the algorithm is presented in Appendix A.

Table 1. Terms and symbols used in the study.

Definition	Symbol	Units	Values/ref.
Peatland area	A	m^2	$9.31 \cdot 10^8$
Elevation of the peat surface	s	m	from DEM
Canal water level measured from the sea level	CWL	m	
Vector representation of the CWL	$\boldsymbol{v}$		
CWL after building a set of blocks	$\boldsymbol{v}'$		
Number of pixels in the canal raster	n		11311
Canal block vector	$\boldsymbol{k}$		Eq.(10)
Number of blocks	b		$0 \dots 80$
Head level of canal block measured from the soil surface	hl	m	0.2 - 0.4
Distance between s and CWL in the absence of any blocks	wd	m	1.2
Water table depth measured from the soil surface	WTD	m	
Spatial average of WTD	ζ	m	Eq.(5)
Temporal average of WTD over three days	$\langle \zeta \rangle$	m	Eq.(7)
Hydraulic head	h	m	
Precipitation	P	mm d^{-1}	0
Evapotranspiration	ET	mm d^{-1}	3
Impermeable bottom: depth of the peat deposit	ib	m	from peat depth raster
Specific yield	S_y		
Hydraulic conductivity	K	m d^{-1}	
Transmissivity	T	m^2 d^{-1}	Eq.(4)
Marginal benefit	MB	m^3	Eq.(17)

2.1.2 Hydrological model

The hydrological model simulates the two dimensional WTD surface for a given configuration of the blocks. From there it computes the target variable of the optimization algorithm, $\langle \zeta \rangle$, defined in Eq.(7). The WTD was solved using the Boussinesq equation, a quasi-3D groundwater flow partial differential equation (PDE) which is computationally much more efficient than

90 solving the full 3D problem, and is a standard groundwater modeling equation for domains wider than they are thick (Bear, 1979; Connorton, 1985; Skaggs, 1980; Koivusalo et al., 2000; Cobb et al., 2017),

$$S_y(h)\frac{\partial h}{\partial t} = \frac{\partial}{\partial x}\left(T(h)\frac{\partial h}{\partial x}\right) + \frac{\partial}{\partial y}\left(T(h)\frac{\partial h}{\partial y}\right) + P - ET, \tag{2}$$

where S_y is the specific yield, T is the transmissivity (m^2 d^{-1}), h is the hydraulic head (m) and $P - ET$ is the difference between the precipitation and evapotranspiration (m d^{-1}). The WTD is related to h as follows,

$$WTD(x,y) = -\left[s(x,y) - h(x,y) \right], \tag{3}$$

where s is the peat surface in meters above sea level. Equation (2) was numerically solved on a horizontal grid with a daily timestep using a finite volume solver (Guyer et al., 2009). Since Eq.(2) is a non-linear PDE, its solution at each timestep was found iteratively so as to ensure numerical stability. The exterior faces of the grid were open water bodies, and Dirichlet -constant head- boundary conditions were applied on them. The value of h at the canal pixels was forced to be equal to v' by adding an implicit source term large enough to completely dominate the matrix diagonal.

In this setup, the transmissivity is given by

$$T(h) = \int\limits_{ib(x,y)}^{h(x,y)} K(x,y,z) dz, \tag{4}$$

where K is the saturated hydraulic conductivity (m d^{-1}) and ib is the impermeable bottom. The layered structure of the peat deposit, whose hydraulic conductivity $K(x,y,z)$ can vary in orders of magnitude along the vertical direction, z, is thus taken into account in $T(h)$. Since published hydraulic property profiles in tropical peat deposits are scarce (Baird et al., 2017), we parameterized the model based on the following:

- The degree of decomposition (fibric, mesic, sappric) affects the hydraulic conductivity. Hydraulic conductivity values for different decomposition stages were adopted from Wösten et al. (2008).

- Hydraulic conductivity decreases exponentially with depth (Koivusalo et al., 2000; Cobb et al., 2017).

- Woody peat is the dominant material in tropical peat deposits. In absence of measured tropical peat water retention characteristics, we used values from boreal woody peats with the same peat type and degree of decomposition (Päivänen, 1973). The van Genuchten function was used to compute the volumetric water content of peat at depth z for each degree of decomposition and h. From the volumetric water content curves, the specific yield, S_y, the amount of water required for a differential increment in WTD elevation, was calculated.

At each timestep, $T(h)$ and $S_y(h)$ were recomputed for each pixel to ensure accurate estimates. Ponding water in fully saturated profiles was neglected and all surface water was removed from the computation, therefore assuming that the typical runoff velocity of water is greater than the infiltration velocity.

All simulations started from a fully saturated landscape, *i.e.*, $WTD = 0.0$m, or equivalently, $h = s$, which may occur after a heavy tropical rainfall event. Thereafter, for the optimization procedure, 3 dry days without any precipitation, $P = 0$mmd^{-1} and $ET = 3$mmd^{-1}, were simulated with a daily timestep. The reason to adopt this particular setup is that the wet initial state

acts as a system reset which, if followed by a period without precipitation, allows for qualitative comparison with observations. The exact number of dry days was decided according to two criteria. On the one hand, the mean of consecutive rainless days during the dry season in a 20 year time window was 3.2 days (data from Pekanbaru Airport, located in the same province as the target area, years 1994-2013). On the other hand, 3 timesteps results in a manageable computation load in the optimization process.

The spatially averaged WTD (m) at the end of each timestep l was defined as

$$\zeta_l = \frac{1}{A} \iint_A WTD_l^*(x,y) \, dxdy, \tag{5}$$

where the integral extends to the whole peatland area, A, and WTD_l^* stands for the solution of Eq.(2) at timestep l. The mean WTD over d days is then given by

$$\langle \zeta \rangle_d = \frac{1}{d} \sum_{l=1}^{d} \zeta_l, \tag{6}$$

where the brackets $\langle \cdot \rangle$ denote temporal average. The average WTD over three days is specially relevant in this work, and in what follows we will denote it without subscripts,

$$\langle \zeta \rangle = \langle \zeta \rangle_3. \tag{7}$$

In order to estimate the annual CO_2 emissions that a given block configuration produces, the WTD for a full year was also simulated. That simulation was also initialized with fully saturated initial conditions, and was made to coincide with a high rainfall event in December 2012. Following Jauhiainen et al. (2012), it was assumed that the yearly emitted amount of CO_2 per hectare, m_{CO_2} (Mg ha^{-1} y^{-1}) is proportional to $\langle \zeta \rangle_{365}$, *i.e.*,

$$m_{CO_2} = \alpha \langle \zeta \rangle_{365} + \beta, \tag{8}$$

with coefficients

$$\alpha = 74.11 \text{ Mg ha}^{-1}\text{m}^{-1}\text{y}^{-1}$$
$$\beta = 29.34 \text{ Mg ha}^{-1}\text{y}^{-1}. \tag{9}$$

The exact values of α and β are important for the CO_2 emission estimation, but they are not relevant for the rest of the results produced in this work, since only the relative values of m_{CO_2} are of interest in the optimization process. Instead, the crucial feature is that the annual average WTD is linearly related to the emitted amount of CO_2. The whole computational scheme is therefore independent of the exact values of α and β, and they are only used at the last stage in order to report the results in units of annual emitted tonnes of CO_2.

2.1.3 Optimization of block positions (SA and GA)

The management question of finding the position of a given number of blocks in such a way that the amount of emitted CO_2 or its proxy, $\langle \zeta \rangle$, is minimized can be formally formulated as follows. Let $\boldsymbol{k} = (k_1, \ldots, k_n)$ be the vector of block positions, such that each i corresponds to a canal pixel in the canal raster, and

$$k_i = 1 \text{ if there is a block in position } i$$
$$k_i = 0 \text{ otherwise.} \tag{10}$$

The objective function $f : \mathbb{R}^n \to \mathbb{R}$

$$f(\boldsymbol{k}) = \langle \zeta \rangle \tag{11}$$

maps a given block setup to $\langle \zeta \rangle$. The objective function $f(\boldsymbol{k})$ is to be minimized subject to the constraint that

$$\sum_i^n k_i = b, \tag{12}$$

where b is the number of blocks to be built. There is no analytic expression for f. Instead, it is a result of combining the canal blocking subroutine with the hydrological model. As pointed out in the Introduction, the design space is discrete and too large for exhaustive search. Moreover, the search space might have many local minima that are not close to the global minimum, so algorithms that only seek local solutions are not useful. Therefore, this problem is only tractable with non-linear, global optimization algorithms.

Given that there exists no guarantee that the process will converge towards the true global minimum of f, the reliability of the optimization procedure benefits from exploring more than one optimization method. Genetic algorithm (GA) and simulated annealing (SA) are stochastic methods that can find the global minimum with high probability and are naturally applicable for the solution of discrete optimization problems (Rao, 2009). In this case, both algorithms start off with some random $\boldsymbol{k}$ composed of b blocks ($b = 0 \ldots 80$), for which the resulting $\langle \zeta \rangle$ is computed. Then, according to some rules specific to the algorithm, another $\boldsymbol{k}$ is proposed. This process is repeated for a fixed number of iterations, the same for all numbers of blocks. Both algorithms tend to favor the configurations that result in a smaller value of the target variable $\langle \zeta \rangle$, but they also have the vital feature of avoiding getting stuck in local minima. In SA this is achieved by allowing disimprovements with certain probability. This probability is controlled by the only parameter, the temperature (a term coming from metallurgy, where the inspiration for it came from), which decreases from an initial maximum value. In GA, on the other hand, the problem is circumvented by evaluating populations of individual $\boldsymbol{k}$ at each iteration or generation. The fittest individuals are passed on to the next iteration according to some rules that include mixing between individuals, also known as *mating*, and some randomness, or *mutations*. The mutation and the mating probabilities are the only parameters of our implementation of the genetic algorithm.

Table 2. Block locating methods and their parameters. The values of the parameters were decided empirically.

Definition	SA	GA	SO	random	rule-based
Number of iterations or generations	6000	6000	250000	2000	
Number of processors	1	10	10	1	
Initial temperature	300				
Final temperature	1				
Single point crossover mating prob.		0.3	0.3		
Mutation probability		0.1	0.1		

The parameters used for both algorithms were fixed by trial and error, and they are shown in Table 2. The authors are aware that parallelizable versions of SA exist (see, *e.g.*, de Souza et al. (2010)), but the wide spread classical single processor algorithm was chosen for this task. GA was run in parallel over 10 processors. With the same number of iterations (or generations), parallelization allows GA to explore 10 times more block configurations in a similar amount of time. SA was implemented by
180 means of the Python package simanneal 0.5.0 (PyPi), and for GA the *eaSimple* algorithm in the DEAP library (Fortin et al., 2012) was used.

This optimization setup is computationally expensive, regardless of the optimization algorithm used. The main bottleneck of the computation is the numerical solution of the Boussinesq equation, Eq.(2). A simpler alternative is to maximize the CWL change,

185 $$\text{CWL change} = \sum_{i \in \text{canal raster}} (v'_i - v_i), \qquad (13)$$

on its own. The CWL change is represented by the blue shaded area in Figure 2. The rationale behind this alternative choice of the target variable is simple: in general, it is to be expected that a higher CWL will lead to wetter peat throughout the area. By completely bypassing the numerical solution of the PDE, this approach would need a fraction of the computational resources required for the full optimization procedure described above, while potentially obtaining a good approximation of the minimum
190 $\langle \zeta \rangle$. SO was implemented by modifying the target variable of GA and was run for 250000 iterations over 10 processors. This amounted to a similar computational effort as for the SA and GA algorithms.

To evaluate the performance of the optimization algorithms we compared the resulting $\langle \zeta \rangle$ against two other ways of positioning blocks: randomized and rule-based. The random block configurations were generated by randomly selecting locations from a uniform distribution. The value of $\langle \zeta \rangle$ from 2000 random block configurations was computed and aggregated into
195 the mean, $\overline{\langle \zeta \rangle}_r$. The rule-based configuration was constructed following standard procedure in the absence of computational tools : the positions of the blocks were decided based on contour line maps and the canal raster (Armstrong et al., 2009). The rule-based positions of the blocks for $b = 10$ are shown in Figure 7(a).

In order to enable a meaningful comparison between different setups, the average WTD resulting from these simulations was normalized with the average WTD in the absence of blocks. *i.e.*,

$$200 \quad \langle \zeta^{(b)} \rangle_{norm} = \frac{\langle \zeta^{(b)} \rangle}{\langle \zeta^{(0)} \rangle}, \tag{14}$$

where $\langle \zeta^{(b)} \rangle$ is the $\langle \zeta \rangle$ resulting from placing b blocks.

In a similar vein, we define the improvement of any block locating method to be

$$I^{(b)} = \left| \langle \zeta^{(0)} \rangle - \langle \zeta^{(b)} \rangle \right|. \tag{15}$$

It measures the simple difference in mean WTD between the reference value, $\langle \zeta^{(0)} \rangle$, and the one resulting from placing b 205 blocks with any of the methods above. In particular,

$$\overline{I}_r^{(b)} = \left| \langle \zeta^{(0)} \rangle - \overline{\langle \zeta^{(b)} \rangle_r} \right| \tag{16}$$

will be used to denote the mean improvement achieved by locating b blocks randomly.

Yet some more insight can be gained by looking at the results in terms of marginal benefits. We define the marginal benefit of building $b + \Delta b$ blocks over b blocks to be

$$210 \quad MB(b) = \frac{\left| \langle \zeta^{(b+\Delta b)} \rangle_{norm} - \langle \zeta^{(b)} \rangle_{norm} \right|}{\Delta b}. \tag{17}$$

The quantities from Eqs.(14)–(17) are used to investigate the performance of all block placing methods in the task of minimizing $\langle \zeta \rangle$ with a fixed number of blocks.

2.2 Study area

The study area was located in Siak, Riau, Indonesia (Figure 3). The area belongs to humid tropical climate; the mean annual 215 temperature is 27°C with very small monthly variation. The mean annual precipitation in the area is 2696 mm, with the rainy season extending from October to April. The rainfall of the wettest month (November) exceeds 300 mm per month, while the driest month (July) receives 120 mm of rainfall. According to long-term weather statistics the mean dry period between the rainfall events during the dry season is 3.2 days and the maximum number of consecutive dry days was 20. Because of the humid climate and its topography, the area is characterized by tropical peatlands: the total area is 1100 km^2, of which 220 peatlands cover 931 km^2. The depth of the peat deposit ranges from 2 to 8 m, the deepest peat deposit being located in the middle of the area, see Figure 4. Approximately 30% of the peat area represents hemic or moderately decomposed peat, and 60% is sappric or highly decomposed peat. The area was drained using canals of about 5 to 8 m metres wide, which are also used for transportation of wood and other products. The total length of the canal network is 1100 km. Typically, the canals are spaced in intervals of 500 m to 1000 m.

(a)

(b)
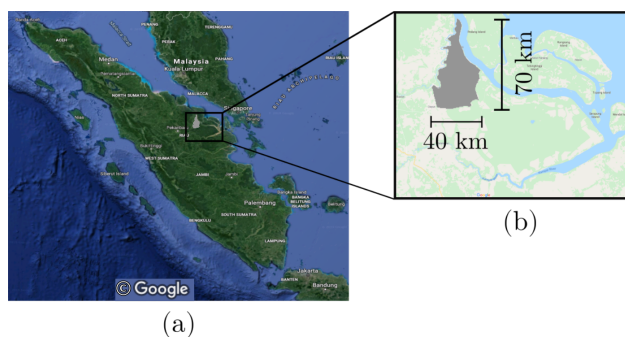
Figure 3. (a) Map of Sumatra Island, Indonesia, with the study area shown in grey. **(b)** Detailed view of the study area. Map data: © Google, Maxar Technologies.


(a)   (b)   (c)
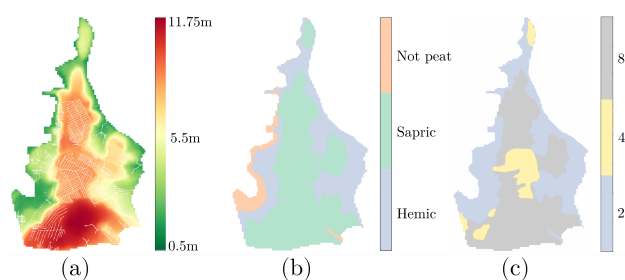
Figure 4. (a) DEM (coloured) with the canal network superposed (white), **(b)** peat types and **(c)** peat depth. The resolution of the rasters is 100 m x 100 m.

225   For our computations we used the 100 m x 100 m resolution raster data shown in Figure 4, which together describe the surface elevation (DEM), the canal location and the peat depth and type. The peat type influenced the peat physical properties, S_y and T, of the hydrological simulation, and the peat depth defines the impermeable bottom ib.

3   Results

3.1   Reality check

230   In order to demonstrate that the hydrological model and the canal water level subroutine reproduce the expected qualitative behaviour of the WTD, two figures are shown. Figure 5 shows the WTD drop during three consecutive dry days for a cross section of the drained area. After three dry days, the WTD drops about 10 cm at the midpoint between two drains separated by 1.4 km. When the canals are closer to each other, WTD drop is larger, and if the canals are far apart the peat remains fully saturated. The shape of the WTD solution between two canals is the typical one for diffusion PDEs such as Eq.(2).

11
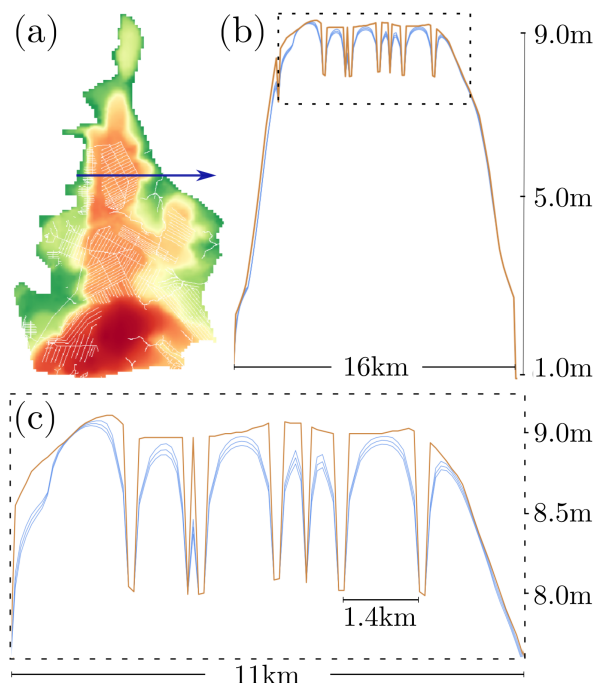
Figure 5. Cross section of the simulated WTD for three consecutive dry days after a big rainfall event. **(a)** DEM (coloured) with the canal network superposed (white) and a straight horizontal line indicating the cross-section area (blue). **(b)** Peat surface (brown) and cross sectional view of the WTD (blue), measured in meters above sea level. Abrupt low peat surface values correspond to canals. The dashed rectangle shows the region amplified in the figure below. **(c)** Magnified area from the figure above.

235   The behaviour of the canal water level subroutine is demonstrated by comparing the CWL change in a small drained area with and without canal blocks (Figure 6). The effect of the canal blocks on the CWL propagates to different distances depending on local topography. If the slope of v is small, the effect of a single block can reach distances of the order of a kilometer. If, instead, v changes very steeply, the effect of a block reaches less far. In addition, the amount of rewetted peat as a consequence of building one block is dependent on the local topography and physical properties of the peat deposit, and on the proximity

240   to other canals. It is precisely the complexity of this response that calls for computational methods in order to solve for the optimal block placement.

3.2   Canal block optimization

The average WTD was computed using different scenarios with increasing number of canal blocks ($b = 5, \ldots, 80$) for each of the block placing methods described (rule-based, random, SA, GA, SO). Their resulting values are shown in Figure 7, and they

245   constitute the main result of the present study.
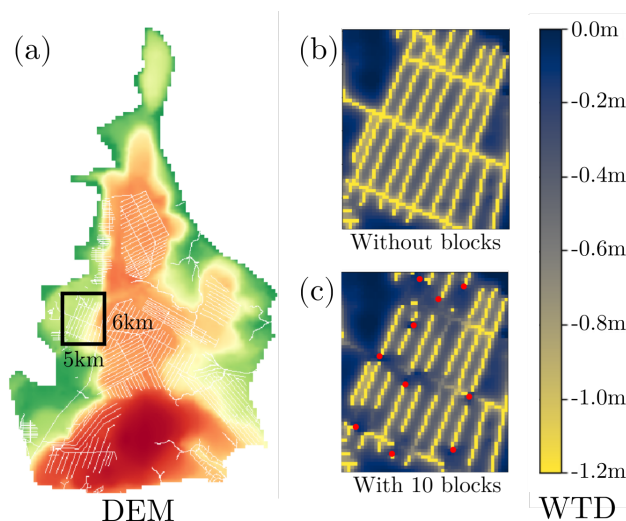
Figure 6. WTD after three dry days with and without blocks. **(a)** DEM (coloured) with the canal network superposed (white) and a rectangle indicating the area shown on the right. **(b)** WTD after three dry days without any blocks. **(c)** WTD after three dry days in the same area with ten blocks (block locations are indicated by red dots). WTD in the canal raster is defined as $\boldsymbol{v}' - \boldsymbol{s}$. Blocks help raise the WTD closer to the surface, but their effectiveness varies from each case depending on the local topography.

The most straightforward observation is that the more blocks there are the larger fraction of peat they will rewet, even if they are placed randomly (Figure 7(b)). The second observation is that the optimization algorithms were able to find systematically better block positions than the random or the rule-based approaches. An informative way to gauge this difference is to realize that they were able to obtain with only 10 blocks the same amount of rewetted peat that the random configurations did with

250   60 blocks. The largest performance difference of the optimization algorithms over the random happened for $b = 5$ and it was approximately $I_{GA}^{(5)} = 7 \cdot \overline{I}_r^{(5)}$ (Figure 7(c)). As the number of blocks increased, $I^{(b)}$ decreased monotonically for every block placement method. For the maximum amount of blocks considered, $b = 80$, $I_{SO}^{(80)} \approx 3 \cdot \overline{I}_r^{(80)}$. That is, at their best, the optimization algorithms were able to find block configurations that rewetted seven times more peat than the random and the rule-based approaches did for the same number of blocks; at their worst, they were three times better than the random.

255   Another thing to note is that the rate at which $\langle \zeta \rangle$ dropped for increasing b was markedly slower for the random block placements than it was for the ones resulting from the optimization algorithms. This can be quantified by the marginal benefit , $MB(b)$ (Figure 7(d)), which gives the slope of Figure 7(b). For clarity, only the MB for the best performing optimized solution is shown. $MB(b)$ for the mean of the random locations was approximately constant, while for the best optimized solution it decreased with b.

260   As Figure 7 shows, GA and SO performed similarly in the task of minimizing $\langle \zeta \rangle$. At first sight, this might look surprising, since the target variable for SO was not $\langle \zeta \rangle$ itself, but the CWL change. In order to understand this behaviour, we need to know how strongly $\langle \zeta \rangle$ and the CWL change are correlated with each other (Figure 8). Figure 8 eloquently displays that the optimal solutions for the two algorithms with $\langle \zeta \rangle$ as a target variable (SA and GA) tend to favour block configurations with smaller
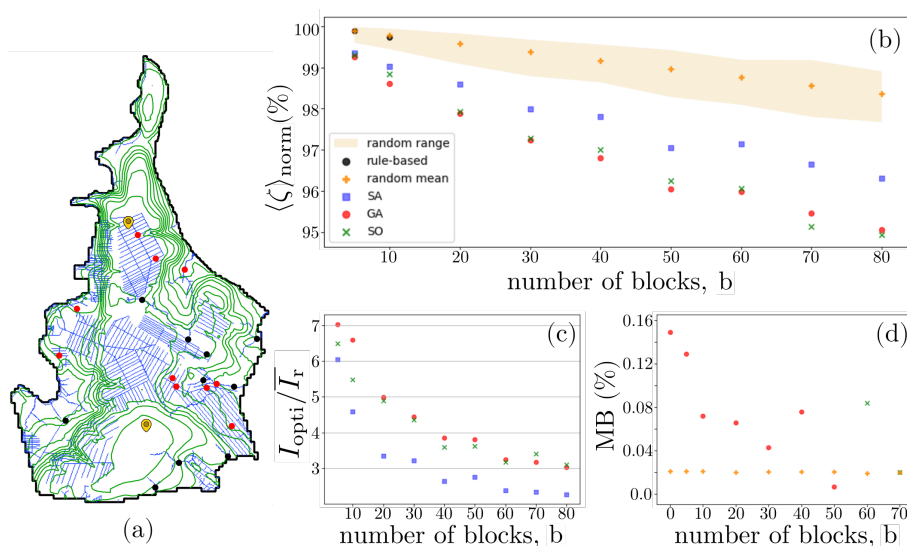
Figure 7. Peat rewetting performance comparison of random block locations, the rule-based approach and the optimization algorithms (SA: simulated annealing; GA: genetic algorithm; SO: simple algorithm) for different numbers of blocks. **(a)** Map of the area. The canal network is shown in blue, and the contour lines in green. The resulting block positions for the case $b = 10$, both for GA (red dots) and rule-based (black dots), are shown. Furthermore, the locations of the annual WTD simulations of Figure 10 are indicated by yellow icons.**(b)** $\langle \zeta \rangle_{norm}$, defined in Eq.(14), as a function of the number of blocks. The random range was linearly interpolated. The rule based approach was only carried out for 5 and 10 blocks. **(c)** Relative improvement of several block locating methods with respect to the mean of the random, as defined in Eq.(16), for different numbers of blocks. **(d)** Marginal benefit, as defined in Eq.(17), for the best performing optimization algorithm and for the mean of the random configurations.

$\langle \zeta \rangle$, regardless of the CWL change, while SO is focused on maximizing CWL change, and gets a good performance in $\langle \zeta \rangle$ as

265   a side product of the correlation between the two.

The sensitivity of $\langle \zeta \rangle$ to the head level of the blocks, hl, is demonstrated in Figure 9, where we plot $\langle \zeta \rangle_{norm}$ resulting from the best available block positions for two different values of the block head level, $hl = \{0.2\,\mathrm{m}, 0.4\,\mathrm{m}\}$. There can be a significant difference in the WTD, especially for large b.

3.3   Implication to CO$_2$ emissions

270   In order to draw further conclusions about the beneficial environmental impact of building canal blocks, we simulated the WTD for a full year under two different regimes: without any blocks and with the best available positions for the maximum number of blocks, 80. Rainfall intensity was taken from Pekanbaru Airport's weather station data, located in the same province as the target area. The big rainfall events registered during December 2012 were used as the starting point for the simulation, which was set up with completely saturated initial conditions. Evapotranspiration was set to $3\,\mathrm{mm\,d^{-1}}$, and the block head

275   level $hl = 0.4\mathrm{m}$. For each of the two block setups three daily WTD time series were recorded: the WTD in a drained area in

14
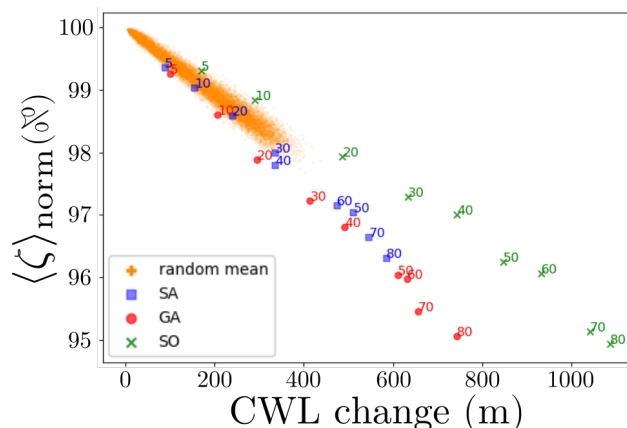
Figure 8. Correlation between $\langle \zeta \rangle$ and the CWL change for the random and the optimized block configurations. The number that accompanies each one of the points stands for b, the number of blocks that were located for each simulation.
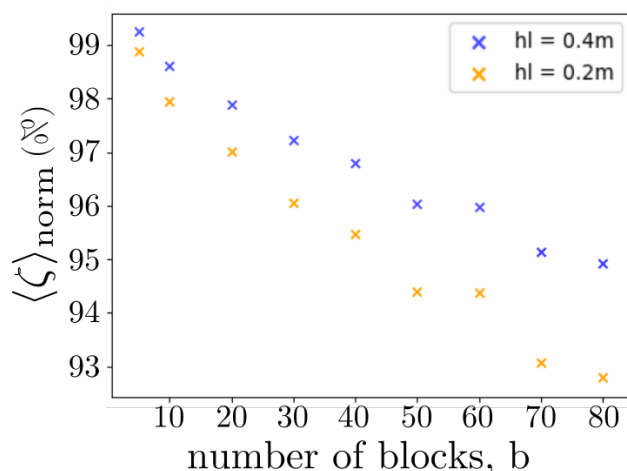

Figure 9. Sensitivity of the average WTD to a difference in the block head level, hl. The values of $\langle \zeta^{(b)} \rangle_{norm}$ correspond to the optimal block positions computed for $hl = 0.2$m (orange) and $hl = 0.4$m (blue).

the north, the WTD in the natural undrained peat dome in the south (Figure 7 (a) shows the exact locations) and the spatially averaged WTD over the whole area, ζ (Figure 10).

Nearby blocks were able to raise the water table by approximately 20 cm in the chosen drained location. In the other end of the spectrum, the WTD in the natural zone was not affected at all. As a result, the effect of the 80 blocks in the WTD over the whole area, given by ζ, was to raise it only by a few cm.

We obtained the following annual average values for the entire area: $\langle \zeta^{(0)} \rangle_{365} = -21.45$ cm without any blocks, and $\langle \zeta^{(80)} \rangle_{365} = -20.08$ cm, with the best available 80 blocks. In order to translate our results about the simulated annual WTD

280

15

Biogeosciences

Discussions

EGU

Open Access
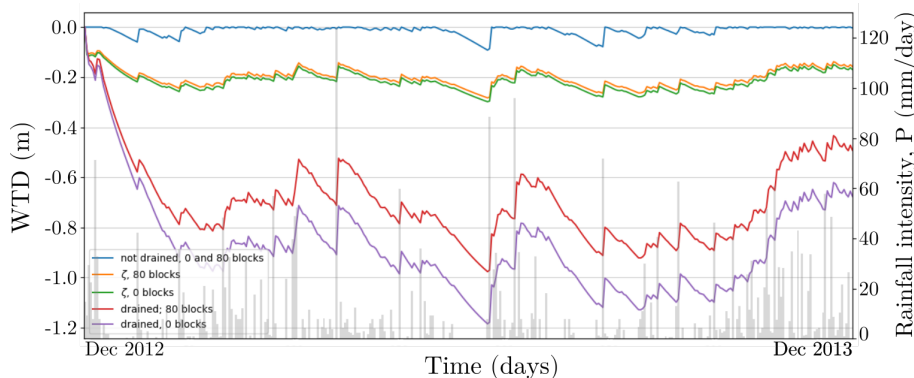
Figure 10. Simulated daily WTD for two sites (drained and natural, see Figure 7 for the exact locations) within the peatland area, and the average WTD, ζ. The same period (December 2012 - December 2013) was simulated without any blocks (green and purple lines) and with the optimized 80 blocks (orange and red lines). The spatial average ζ for $b = \{0, 80\}$ is shown in orange and green. There was no appreciable difference in WTD in the undrained area between different block configurations, and the WTD is shown by a single line (blue line). Daily rainfall intensity is shown as grey vertical lines (data from Pekanbaru airport).

into the amount of emitted CO_2, we used Eq.(8). Thus, $m_{CO_2}^{(0)} = 45.34$ Mg ha^{-1} y^{-1} and $m_{CO_2}^{(80)} = 44.22$ Mg ha^{-1} y^{-1} were obtained for the aforementioned block configurations.

4 Discussion

4.1 Model evaluation and reality check

To the best of our knowledge, this work introduces the first systematic tool that can quantify the rewetting performance of different block configurations. It operates on all the easily available data (weather and GIS-derived data) and combines it in a scientifically coherent way. It is also designed to be computationally feasible for large areas. Therefore, this tool can potentially be very useful for decision makers in greenhouse gas emission mitigation and drained peatland restoration contexts.

The qualitative behaviour of the WTD and of the CWL in Figures 5 and 6 reflect the following expected traits. First of all, WTD lowers with time as a result of drainage. Second, the smaller the distance between canals, the more the WTD drops, for it was assumed that the system lacks any water input. In contrast, the WTD might stay close to the surface if the canals are far apart enough. Moreover, the effect of a set of blocks in the CWL propagates upstream in the correct way.

In this study we did not validate the hydrological model against actual field data, because there is no extensive, publicly available dataset. The aim of the paper was not to test a new hydrological model *per se*, but rather to solve a management question by applying a pre-existing one with parameter values derived from literature. We assume that a more precise parameterization would not have changed the outcome of the optimization procedure, and thus the qualitative assessment of the parameters' fitness was enough to fulfil our principal objective. It might be argued that in the absence of a quantitative validation, there

300   is a high uncertainty in the simulated annual WTD in Figure 10. For instance, if 80 blocks were built in the best available
positions so that their head level was only 20 cm higher, then the three-day average of the WTD would be 2.13% units lower
(*c.f.* Figure 9). However, the simulated daily WTD of Figure 10 are in the same range and show similar dynamics as those
reported earlier for drained peatlands in similar areas (Jauhiainen et al., 2012; Hooijer et al., 2012; Evans et al., 2019), and for
natural peatland forests in Great Sunda islands (Cobb et al., 2017; Evans et al., 2019). Thus, we assume that WTD in Figure
305   10 and the consecutive CO_2 emissions, discussed in section 4.3, are plausible.

Some remarks about the assumptions made in the canal water level subroutine are in order. As explained in section 2.1.1,
the CWL in the absence of blocks was inferred from the DEM using a constant wd (see Eq.(1)). This implies that any local
fluctuation in the height of the DEM is directly transferred to the CWL. Indeed, a CWL derived in this manner is not expected
to be monotonically decreasing in the direction of water flow. Given the nature of the canal water level subroutine, the non-
310   monotonic nature of the CWL can lead to incorrect predictions of the effect a block has on the CWL. Another source of
misrepresentation of the connectivity of the CWL comes from the artifact that the resolution of the DEM, 100 m x 100 m,
introduces. According to the rules in section 2.1.1, if two different canals happen to be less than 100 m apart, then rule 1 will
erroneously infer that those two pixels are in direct causal contact. These problems could be ameliorated by using a separate
canal network vector layer which contains the direction of the water flow. There is yet another class of approximations that were
315   made in Eq.(1). First of all, in reality wd is not constant but it might vary in time due to seasonality, and in space at different
heights. It is also worth noting that the resulting water profile after building a block is typically not a perfectly horizontal line,
as depicted with dotted lines in Figure 2, but an inclined one. Furthermore, we are implicitly neglecting tidal effects, which
could affect the water flow direction close to the seashore. All these approximations were either imposed by the quality of the
data or judged to be of secondary importance in the computation of the CWL.

320   ## 4.2   Canal block optimization

Two basic observations can be drawn from Figure 7. The first is that the performance of the rule-based approach is comparable
to that of random location of the blocks. The positions for the blocks in the rule-based approach were based on the contour
line map of Figure 7(a). Figure 7(a) makes it apparent that it is very difficult to predict the effect of the blocks on the WTD
by using logical reasoning alone: there are no evident differences between the locations of the blocks placed according to the
325   rule-based and the GA methods. The rule-based approach was only carried out for 5 and 10 blocks, yet, as b increases so does
the complexity of the task, and it is therefore not expected that it would perform any differently from the random method when
the amount of blocks increased. This leads us to conclude that the combination of the random trials and the rule-based approach
may be interpreted as the best humanly possible results in the absence of any computational tools.

The second observation is that the optimization algorithms performed systematically better than the random and rule-based
330   approaches. Going into further details, GA and SO were more successful in minimizing $\langle \zeta \rangle$ than SA. Under the same condi-
tions, GA and SA are expected to perform similarly (Rao, 2009), but the single processor nature of SA restricted its search
space to be 10 and 417 times smaller than those of GA and SO, respectively. The optimization performance of GA and SO was
very similar for all numbers of blocks, but SO performed best for higher numbers of blocks. Both strategies are sound from

the hydrological point of view, but their success in the optimization happen for different reasons. The good performance of SO

335   can be explained by two factors. On the one hand, its simplicity allowed it to explore 42 times more block configurations than GA, thus being able to reach a fairly good approximation of the maximum CWL change even for large b. On the other hand, $\langle \zeta \rangle$ and the CWL change correlated strongly as is shown in Figure 8, meaning that SO got a good result in $\langle \zeta \rangle$ minimization as a byproduct of CWL change maximization. Another way of putting this is that, unlike the CWL change, $\langle \zeta \rangle$ gets the full 3D information about the catchment topography and the peat physical properties, but in return, the optimization task is heavier.

340   This may not be true for any study area. For instance, in domains with high spatial heterogeneity in peat physical properties the correlation is expected to be less evident. As the number of blocks to locate, b, increases, the size of the search space does so as $\binom{n}{b}$. It is this exponential increase in computational complexity what might explain the better performance of SO when the number of blocks is greater. Following this line of reasoning, the fact that SO performs better than GA only for $b = \{70, 80\}$ leads us to conclude that computational resources are limiting the performance of GA at least at those values of b, *i.e.*, a sub-

345   stantially better performance of GA is to be expected for high b if the number of iterations increased. The success of both GA and SO calls for an alternative optimization strategy that would profit from both algorithm's strengths. Such an algorithm could be designed so that GA was initialized with several optima from the fast SO.

        However interesting, comparing the performance of different algorithms was not the objective of this work. Instead, the main conclusion can be drawn by contrasting the outcome of the optimization algorithms with the best humanly available

350   guesses. With the same number of blocks, the reduction in average WTD by the optimized block configuration is systematically greater than the one achieved simply by logical reasoning (Ritzema et al., 2014; Armstrong et al., 2009). This contrast is most significant for a small number of blocks, where the average WTD reduction resulting from the best available block locations is up to 7 times larger than the one derived from the mean of the random blocks (Figure 7(c)). As the number of blocks increases the relative improvement I decreases, likely due to two main reasons. On the one hand, the aforementioned difficulty for the

355   algorithms to find the optimal solution in an increasingly larger search space. On the other hand, the fact that the best positions might already be occupied by some of the blocks.

        Another metric of interest to compare different block locating methods is the marginal benefit of adding one more block, shown in Figure 7(d). The marginal benefit for the random block configurations was almost constant, *i.e.*, the decrease of $\langle V_r^{(d)} \rangle$ was linear. This implies that if the blocks were to be built randomly, each additional block would be equally successful

360   in reducing $\langle \zeta \rangle$. In contrast, the marginal benefit for the best available block locations varied with the number of blocks. Overall, it decreased as the number of blocks increased. This implies that the benefit of adding one more block decreases with the number of blocks that are already built. This fact is, once again, likely due to the two factors mentioned above. On the one hand, it is increasingly difficult for the algorithms to find an optimal solution in an exponentially increasing search space. On the other hand, for large number of blocks the most beneficial block locations are already occupied. Theoretically, there

365   exists a limiting number of blocks at which the finite size of the area would make the marginal benefit to decrease even with the absolute best block locations. We suspect that with the current b we were not yet at the limits of the system and that this finite-size phenomena will only be relevant for larger b.

It is not expected that a different choice of parameters would affect these general observations about the optimization results. While different parameterizations will result in a different WTD in absolute terms (see, *e.g.*, the case of hl, Figure 9), the relative
370 differences in WTD between all block locating methods remain for different choices of parameter values. It is also worth mentioning that solving the steady-state version of the Boussinesq equation, Eq. (2), was explored as the way to compute the target variable of the optimization, $\langle\zeta\rangle$. However, this approach was discarded in favour of the presented transient equation due to two observations. First, the steady-state solution does not yield a proper description of groundwater behaviour. In tropical climates rainfall is a key driver of hydrological processes and rainfall intensity is all but uniform in time. Thus forcing the
375 model to run with average rainfall and evapotranspiration does not result in a satisfactory model of these systems. Second, the computational time needed to solve the steady-state version, a decisive quantity to obtain an efficient performance in the optimization routine, was comparable to the time needed to solve the transient equation. This stems from the fact that Eq.(2) is a non-linear PDE (both S_y and T depend on h), and in order to ensure numerical stability iterative approximations of the solution are needed even when solving the steady-state problem.

380 ### 4.3 Implication to CO_2 emissions

The simulated annual CO_2 emissions of section 3.3 are within the range of the values in the literature for peatlands in the same region (Hooijer et al., 2012; Evans et al., 2019). Relatively speaking, building 80 blocks to the whole 931 km^2 area mitigates only 2.24% of the CO_2 emissions. The reason for this modest performance might lie in 80 being too few blocks for such a large area. Let us note that there are approximately 1100 km of canals. When placing 80 blocks, the expected distance between
385 a pair of blocks is about 14 km. Yet the influence a block has on the CWL spans, in our study area, a maximum of 2km. We may stretch our results further to give a rough estimate of the number of blocks needed in order to prevent 10% of the emissions in the study area. Taking the values for 80 blocks as a reference, and assuming that $\langle\zeta^{(b)}\rangle$ decreases linearly with b, 350 blocks would be needed to reach that emission reduction goal. This would correspond to having on average one block every three kilometres. Of course, assuming that $\langle\zeta^{(b)}\rangle$ decreases linearly with b is only a rough approximation (Figure 7 shows
390 the true dependence). This leads to the second reason for the modest performance of the 80 blocks: there seems to be room for improvement in our optimization procedure.

On the other hand, looking at the CO_2 emissions in absolute terms, 1.01 tonnes per hectare, or a total of 94156 tonnes throughout the whole area are prevented annually by building 80 blocks. To get a grasp of the magnitude of these numbers, they are of the order of what 25000 cars with a mileage of 20000 kilometres per year would emit.

395 ### 5 Conclusions

We constructed an optimization scheme that looks for the maximum water table raise for a drained peatland area given a fixed amount of canal blocks. Our results show that, with the same amount of resources (*i.e.*, number of blocks) the present computational setup enables a more effective canal blocking restoration of drained peatlands than human guesses do. The computational approach also enables cost-benefit analysis to solve several management questions.

400 *Code and data availability.* The source code and the data used are available under the MIT license at https://github.com/LukeEcomod/blopti.

(Urzainki, 2020)

Appendix A: Canal water level subroutine

The information about the topology of the canal network was stored in a (sparse) matrix, M, of dimensions $(n \times n)$, where n is the number of pixels in the canal raster. For any two pixels of the canal raster, i and j , the entries of the matrix M are

405 $M_{ij} = 1$, if i is in direct causal contact with j

$M_{ij} = 0$ otherwise,   (A1)

where the connectivity conditions are given in rules 1 and 2 of section 2.1.1. Note in particular that if $M_{AB} = 1$, that is, pixels A and B are in direct causal contact and pixel B is upstream, it follows that $M_{BA} = 0$. Moreover, note that $M_{ii} = 0$ for any i. In other words, M is not symmetrical and all the elements of its diagonal are equal to zero. M can then be interpreted as the

410 adjacency matrix of the simple, directed graph G whose nodes are the pixels of the canal raster and an edge exists if two nodes are in direct physical contact (Newman, 2018). In such a graph, the direction of the edges is the opposite to the direction of the water flow. Within this setup, the vector $\boldsymbol{k}' = \boldsymbol{k}M$, where $\boldsymbol{k}$ is the vector of the blocks' positions defined in Eq.(10), contains the information about all the first neighbours of the blocks in $\boldsymbol{k}$. Specifically,

$k'_j = k_i M_{ij} = 1$, if pixel j is in direct causal contact with a block situated in pixel i

415 $k'_j = k_i M_{ij} = 0$ otherwise.   (A2)

Say we wish to build a block in pixel A, that is, $k_i = 1$ only for $i = A$. The operations that the canal water level subroutine performs in order to propagate the effect of this block to the neighbouring nodes of A are described in Algorithm 1.

Algorithm 1 Single iteration in the computation of $\boldsymbol{v}'$ from a $\boldsymbol{k}$ that consists of a single block in pixel A.

1: $v'_A \leftarrow v_A + hl$

2: $k' \leftarrow kM$

3: **for** j in canal raster **do**

4:      **if** $k'_j = 1$ **and** $v_j < v'_A$ **then**

5:          $v'_j \leftarrow v'_A$.

6:      **end if**

7: **end for**

Line 1 sets the new value of the CWL in the pixel were the block is built to be lh units higher. In line 2 the neighbouring pixels that are in causal contact with pixel A are stored into $\boldsymbol{k}'$. The two conditions in line 4 effectively implement rules 1 and

420 2 of section section 2.1.1. Finally, for those pixels for which these two conditions are met, the CWL gets updated.

For the sake of readability, Algorithm 1 shows a single step in the process of computing v', *i.e.*, it only updates the CWL for the first upstream pixels of a block located in A. In order to obtain the final CWL, the operations in Algorithm 1 would have to be iterated over for all successive v' until no more pixels were affected in the canal network. The algorithm could also be extended straightforwardly to any number of blocks. Following these rules, the CWL obtained after building a block looks like

425   the one in Figure 2.

Author contributions. IU and AL contextualized the problem and developed the model code. IU performed the simulations. AB, IB and MN produced and validated the datasets. KH helped formulating research goals and methods. MP, HH and AL contributed with reviewing and editing the text. IU prepared the manuscript with contributions from all co-authors.

Competing interests. The authors declare that they have no conflict of interest

References

Armstrong, A., Holden, J., Kay, P., Foulger, M., Gledhill, S., Mcdonald, A. T., and Walker, A.: Drain-blocking techniques on blanket peat : A framework for best practice, Journal of Environmental Management, 90, 3512–3519, https://doi.org/10.1016/j.jenvman.2009.06.003, 2009.

435 Baird, A. J., Low, R., Young, D., Swindles, G. T., Lopez, O. R., and Page, S.: High permeability explains the vulnerability of the carbon store in drained tropical peatlands, Geophysical Research Letters, 44, 1333–1339, https://doi.org/10.1002/2016GL072245, 2017.

Bear, J.: Hydraulics of Groundwater, McGraw-Hill Series in Water Resources and Environmental Engineering, 1979.

Cobb, A. R., Hoyt, A. M., Gandois, L., Eri, J., Dommain, R., Salim, K. A., Kai, F. M., Su'ut, N. S. H., and Harvey, C. F.: How temporal patterns in rainfall determine the geomorphology and carbon fluxes of tropical peatlands, PNAS, 114, E5187–E5196, 440   https://doi.org/10.1073/pnas.1701090114, 2017.

Connorton, B. J.: Does the regional groundwater-flow equation model vertical flow?, Journal of Hydrology, 79, 279–299, https://doi.org/10.1016/0022-1694(85)90059-9, 1985.

de Souza, S. X., Suykens, J. A. K., Vandewalle, J., and Bollé, D.: Coupled Simulated Annealing, IEEE Transactions on Systems, Man, and Cybernetics, Part B (Cybernetics), 40, 320–335, 2010.

445 Dunn, S. and Mackay, R.: Modelling the hydrological impacts of open ditch drainage, Journal of Hydrology, 179, 37–66, https://doi.org/10.1016/0022-1694(95)02871-4, 1996.

Evans, C. D., Williamson, J. M., Kacaribu, F., Irawan, D., suardiwerianto, Y., M F Hidayat, A. L., and Page, S. E.: Rates and spatial variability of peat subsidence in Acacia plantation and forest landscapes in Sumatra, Indonesia, Geoderma, 338, 410 – 421, https://doi.org/10.1016/j.geoderma.2018.12.028, 2019.

450 Fortin, F.-A., De Rainville, F.-M., Gardner, M.-A., Parizeau, M., and Gagné, C.: DEAP: Evolutionary Algorithms Made Easy, Journal of Machine Learning Research, 13, 2171–2175, 2012.

Guyer, J. E., Wheeler, D., and Warren, J. A.: FiPy: Partial Differential Equations with Python, Computing in Science Engineering, 11, 6–15, 2009.

Holden, J.: Peatland hydrology and carbon release: why small-scale process matters, Philosophical Transactions of the Royal Society A: 455   Mathematical, Physical and Engineering Sciences, 363, 2891–2913, https://doi.org/10.1098/rsta.2005.1671, 2005.

Holden, J., Evans, M. G., Burt, T. P., and Horton, M.: Impact of land drainage on peatland hydrology, Journal of Environmental Quality, 35, 1764 – 1778, 2006.

Hooijer, A., Page, S., Canadell, J. G., Silvius, M., Kwadijk, J., Wösten, H., and Jauhiainen, J.: Current and future CO_2 emissions from drained peatlands in Southeast Asia, Biogeosciences, 7, 1505–1514, https://doi.org/10.5194/bg-7-1505-2010, 2010.

460 Hooijer, A., Page, S., Jauhiainen, J., Lee, W. A., Lu, X. X., Idris, A., and Anshari, G.: Subsidence and carbon loss in drained tropical peatlands, Biogeosciences, 9, 1053–1071, https://doi.org/10.5194/bg-9-1053-2012, 2012.

Jauhiainen, J., Hooijer, A., and Page, S. E.: Carbon dioxide emissions from an Acacia plantation on peatland in Sumatra, Indonesia, Biogeosciences, 9, 617–630, 2012.

Jin, X., Pukkala, T., and Li, F.: Fine-tuning heuristic methods for combinatorial optimization in forest planning, European Journal of Forest 465   Research, 135, 765–779, 2016.

Koivusalo, H., Karvonen, T., and Lepistö, A.: A quasi-three dimensional model for predicting rainfall-runoff processes in a forested catchment in Southern Finland, Hydrology and Earth System Sciences, 4(1), 65–78, 2000.

Laurén, A., Asikainen, A., Kinnunen, J.-P., Palviainen, M., and Sikanen, L.: Improving the financial performance of solid forest fuel supply using a simple moisture and dry matter loss simulation and optimization, Biomass and Bioenergy, 116, 72–79, 2018.

470 Minkkinen, K. and Laine, J.: Long-term effect of forest drainage on the peat carbon stores of pine mires in Finland, Canadian Journal of Forest Research, 28(9), 1267–1275, https://doi.org/10.1139/x98-104, 1998.

Newman, M.: Networks, Oxford University Press, 2 edn., 2018.

Nieminen, M., Sallantaus, T., Ukonmaanaho, L., and Sarkkola, S.: Nitrogen and phosphorus concentrations in discharge from drained peatland forests are increasing, Science of the Total Environment, 609, 974–981, https://doi.org/10.1016/j.scitotenv.2017.07.210, 2017.

475 Ojanen, P., Minkkinen, K., Alm, J., and Penttilä, T.: Soil-atmosphere CO2, Ch4 and N2O fluxes in boreal forestry-drained peatlands, Forest Ecology and Management, 260, 411–421, https://doi.org/10.1016/j.foreco.2010.04.036, 2010.

Page, S. E., Rieley, J. O., and Banks, C. J.: Global and regional importance of the tropical peatland carbon pool, Global Change Biology, 17, 798–818, https://doi.org/10.1111/j.1365-2486.2010.02279.x, 2011.

Päivänen, J. and Hånell, B.: Peatland Ecology and Forestry -A Sound Approach, University of Helsinki Department of Forest Sciences
480 Publications 3, 2012.

Parry, L. E., Holden, J., and Chapman, P. J.: Restoration of blanket peatlands, Journal of Environmental Management, 133, 193–205, 2014.

PyPi: Simulated Annealing in Python, https://pypi.org/project/simanneal/, accessed: December 2019.

Päivänen, J.: Hydraulic conductivity and water retention in peat soils, Acta Forestalia Fennica, 129, 1973.

Rao, S. S.: Engineering Optimization -Theory and Practice, John Wiley & Sons, 2009.

485 Reddy, K. R. and DaLaune, R. D.: Biogeochemistry of Wetlands, CRC Press, 2008.

Ritzema, H., Limin, S., Kusin, K., Jauhiainen, J., and Wösten, H.: Canal blocking strategies for hydrological restoration of degraded tropical peatlands in Central Kalimantan, Indonesia, Catena, 114, 11–20, 2014.

Skaggs, R. W.: A water management model for artificially drained soils, Technical Bulletin, North Carolina Agricultural Experiment Station, 267, 54pp., 1980.

490 Urzainki, I.: blopti- canal blocking optimization, https://doi.org/10.5281/zenodo.3741043, 2020.

Wilson, L., Wilson, J., Holden, J., Johnstone, J., Armstrong, A., and Morris, M.: Ditch blocking, water chemistry and organic carbon flux: Evidence that blanket bog restoration reduces erosion and fluvial carbon loss, Science of the Total Environment, 409, 2010–2018, 2011.

World Resources Institute: Climate Watch, https://www.climatewatchdata.org, accessed: June 2019.

Wösten, J. H. M., Clymans, E., Page, S. E., Rieley, J. O., and Limin, S. H.: Peat-water interrelationships in a tropical peatland ecosystem in
495 Southeast Asia, Catena, 73, 212–224, 2008.

Xu, J., Morris, P. J., Liu, J., and Holden, J.: PEATMAP: Refining estimates of global peatland distribution based on a meta-analysis, Catena, 160, 134–140, 2018.